Supporting information

Non-linear optical-dielectric duple switch and narrow band gap in a one-dimensional hybrid compound: $[(CH_3)_2S(CH_2)_3NH_3][SbBr_5]$

Peng-Peng Gong, Qian-Jun Gu, Ya-Juan Li, Yi Guo, Wan-Yu Zhu and Bo Huang*

Yunnan Key Laboratory of Modern Separation Analysis and Substance Transformation, College of Chemistry and Chemical Engineering, Yunnan Normal University, Kunming 650500, China.

Contents

Ultraviolet-vis spectrum. The generated reflectance-versus-wavelength data were used to estimate the band gap of the material by converting reflectance data to absorbance according to the Kubelka-Munk function:

$$F(R_\infty) = (1 - R_\infty)^2 / 2R_\infty$$

The optical band gap can be determined by the variant of Tauc equation:

$$\left(h\nu \cdot F(R_\infty)\right)^{1/n} = A(h\nu - E_g)$$

where h is Planck's constant, ν is the vibrational frequency, $F(R_\infty)$ is the Kubeka-Munk equation, E_g is the band gap, and A is a material-dependent proportionality constant. The value of the exponent *n* denotes the nature of the sample transition. For direct allowed transition, n = 1/2; for indirect allowed transition, n = 2. Hence, the optical band gap E_g can be obtained from a Tauc plot by plotting $\left(h\nu \cdot F(R_\infty)\right)^{1/n}$ against the energy in eV and extrapolation of the linear region to the X-axis intercept.

Calculation of Band Structure. We perform first-principles calculations based on density functional theory (DFT) as implemented in the PWmat package with GPU acceleration.[1-3] The exchange-correlation potential is treated within the generalized gradient approximation (GGA) using the Perdew–Burke–Ernzerhof (PBE) function,[4,5] which is employed for both geometry optimization and band structure calculations. Geometry optimization is carried out with a force convergence criterion of 0.02 eV/Å for the maximum residual force. A Monkhorst–Pack k-point mesh of 1×2×2 is used for geometry optimization, while a denser mesh of 3×6×4 is adopted for self-consistent field and density of states calculations. The self-consistent calculations are converged with an energy threshold of 10^{-6} eV. Norm-conserving pseudopotentials are applied with a cutoff energy of 70 Rydberg for geometry optimization and 60 Rydberg for band structure and density of states calculations.[6]

Table S1. Summary of crystal data and structural refinements of **1** at 100 and 303 K.

Empirical formula	$[(CH_3)_2S(CH_2)_3NH_3][SbBr_5]$	
Formula weight	642.54	
Phase type	LTP	HTP
T / K	100(2)	303(2)
Space group	$Pca2_1$	$Pcmn$
a / Å	25.1840(6)	12.7383(6)
b / Å	8.0686(2)	8.1702(4)
c / Å	15.1437(4)	15.2713(8)
V / Å^3	3077.2(1)	1589.4(1)
Z	4	2
D_{calcd} / g cm^{-3}	2.774	2.685
μ / mm^{-1}	14.881	14.405
GOF	1.006	1.116
R_1, wR_2 [$I > 2\sigma(I)$][a]	0.0241, 0.0448	0.0442, 0.0909
R_1, wR_2 (all data)	0.0276, 0.0456	0.0967, 0.1052
Flack parameter	0.497(9)	–
CCDC *No.*	2526236	2526235

[a] $R_1 = F_o - F_c / F_o$, $wR_2 = \{w[(F_o)^2 - (F_c)^2]^2 / w[(F_o)^2]^2\}^{1/2}$

Table S2. The selected bond lengths (Å) of **1** at 100 and 303 K.

100 K	Sb1–Br1	2.6484(9)	Sb1–Br2	2.8084(9)
	Sb1–Br3	2.7109(8)	Sb1–Br4	2.8015(9)
	Sb1–Br5	2.9166(9)	Sb1–Br6	2.9778(9)
	Sb2–Br6	3.0378(8)	Sb2–Br7	2.9165(9)
	Sb2–Br8	2.6872(9)	Sb2–Br9	2.6006(8)
	Sb2–Br10	2.6435(8)		
303 K	Sb1–Br1	3.0292(4)	Sb1–Br1[1]	3.0292(4)
	Sb1–Br2	2.867(1)	Sb1–Br3	2.6489(7)
	Sb1–Br3[2]	2.6489(7)	Sb1–Br4	2.728(1)

Symmetry code: [1]-1-x, 1/2+y, 1-z; [2]+x, 3/2-y, +z

Table S3. The selected bond angles (°) of **1** at 100 and 303 K.

100 K	∠Br1–Sb1–Br2	90.01(3)	∠Br1–Sb1–Br3	93.53(3)
	∠Br1–Sb1–Br4	91.87(3)	∠Br1–Sb1–Br5	90.97(3)
	∠Br1–Sb1–Br6	177.85(3)	∠Br2–Sb1–Br5	92.64(2)
	∠Br2–Sb1–Br6	91.16(2)	∠Br3–Sb1–Br2	89.11(3)
	∠Br3–Sb1–Br4	90.54(3)	∠Br3–Sb1–Br5	175.18(3)
	∠Br3–Sb1–Br6	88.29(2)	∠Br4–Sb1–Br2	178.10(3)
	∠Br4–Sb1–Br5	87.57(3)	∠Br4–Sb1–Br6	86.97(2)
	∠Br5–Sb1–Br6	87.18(3)	∠Br7–Sb2–Br6	90.61(2)
	∠Br8–Sb2–Br6	87.25(2)	∠Br8–Sb2–Br7	175.88(3)
	∠Br9–Sb2–Br6	90.84(2)	∠Br9–Sb2–Br7	90.34(3)
	∠Br9–Sb2–Br8	93.22(3)	∠Br9–Sb2–Br10	92.43(3)
	∠Br10–Sb2–Br6	176.50(3)	∠Br10–Sb2–Br7	90.60(3)
	∠Br10–Sb2–Br8	91.34(3)	∠Sb1–Br6–Sb2	164.07(3)
303 K	∠Br1–Sb1–Br1^{1}	84.80(1)	∠Br1–Sb1–Br2	89.57(2)
	∠Br1^{1}–Sb1–Br2	89.57(2)	∠Br1–Sb1–Br3	175.93(2)
	∠Br1^{1}–Sb1–Br3	91.26(2)	∠Br1–Sb1–Br3^{2}	91.26(2)
	∠Br1^{1}–Sb1–Br3^{2}	175.93(2)	∠Br1–Sb1–Br4	89.28(2)
	∠Br1^{1}–Sb1–Br4	89.28(2)	∠Br2–Sb1–Br3	89.36(3)
	∠Br2–Sb1–Br3^{2}	89.36(3)	∠Br2–Sb1–Br4	178.44(4)
	∠Br3–Sb1–Br3^{2}	92.65(4)	∠Br3–Sb1–Br4	91.72(3)
	∠Br3^{2}–Sb1–Br4	91.72(3)	∠Sb1–Br1–Sb1^{3}	180

Symmetry code: ^{1}-1-*x*, 1/2+*y*,1-*z*; ^{2}+*x*, 3/2-*y*, +*z*; ^{3}-1-*x*, 1-*y*, 1-z

Table S4. The geometry (Å, °) of hydrogen bonds for **1** at 100 K and 303 K.

	D–H···A	D–H	H···A	D···A	∠D–H···A
100 K	N1-H1A···Br4	0.910	2.740	3.396	129.85
	N1-H1A···Br6	0.910	2.858	3.569	136.06
	N1-H1B···Br1[1]	0.910	2.741	3.463	137.05
	N1-H1B···Br3[1]	0.910	2.759	3.411	129.53
	N1-H1C···Br8[2]	0.910	2.659	3.540	163.22
	N2-H2C···Br2[3]	0.910	2.480	3.368	165.14
	N2-H2D···Br3[3]	0.910	2.949	3.594	129.24
	N2-H2D···Br5[4]	0.910	2.973	3.466	115.70
	N2-H2D···Br6[3]	0.910	2.994	3.416	110.10
	N2-H2E···Br7[3]	0.910	2.482	3.387	172.64
303 K	N1-H1A···Br3[5]	0.890	2.509	3.397	176.21
	N1-H1B···Br2	0.890	2.605	3.353	142.28
	N1-H1C···Br1	0.890	2.599	3.371	145.60

Symmetry code: [1]-*x*+1, -*y*+1, *z*+1/2; [2]*x*, *y*-1, *z*; [3]*x*, *y*-1, *z*+1; [4]*x*, *y*, *z*+1; [5]-*x*-3/2, -*y*+3/2, *z*-1/2;

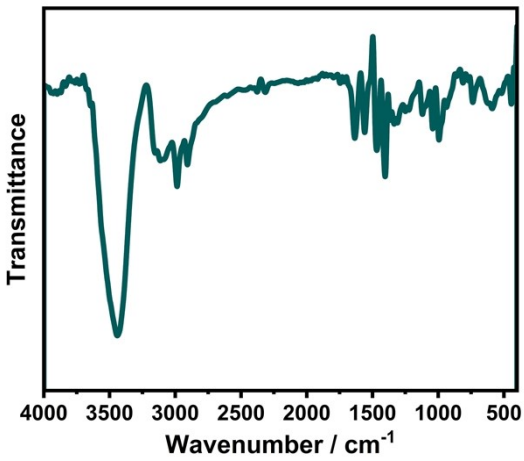

Fig. S1 Infrared spectrum of **1**. The peaks observed at 3441 cm^{-1}, 3113 cm^{-1}, and 1119 cm^{-1} could be attributed to the stretching vibrations of N–H, C–H, and C–N, respectively. The peaks observed at 1634 cm^{-1}, 1467 cm^{-1}, and 1403 cm^{-1} could be assigned to the bending vibration of N–H, $–CH_3$, and $–S(CH_3)_2$, respectively. The peaks observed at 736 cm^{-1} could be attributed to the stretching vibrations of C–S.

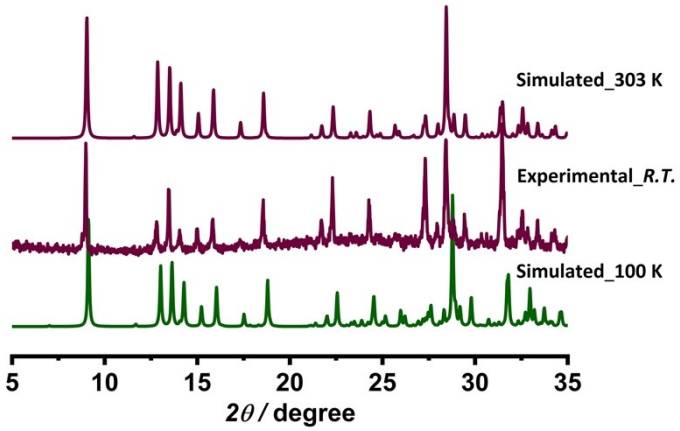

Fig. S2 The simulated (100 and 303 K) and experimental powder XRD patterns of **1**.

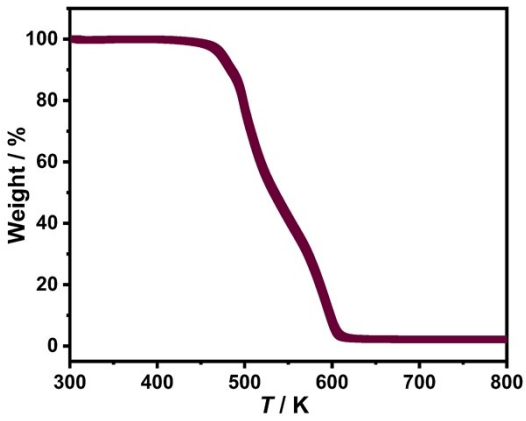

Fig. S3 Thermogravimetric curve measured at a rate of 5 K min^{-1} under N_2 atmosphere of **1**. It reveals that compound **1** was stable up to about 430 K.

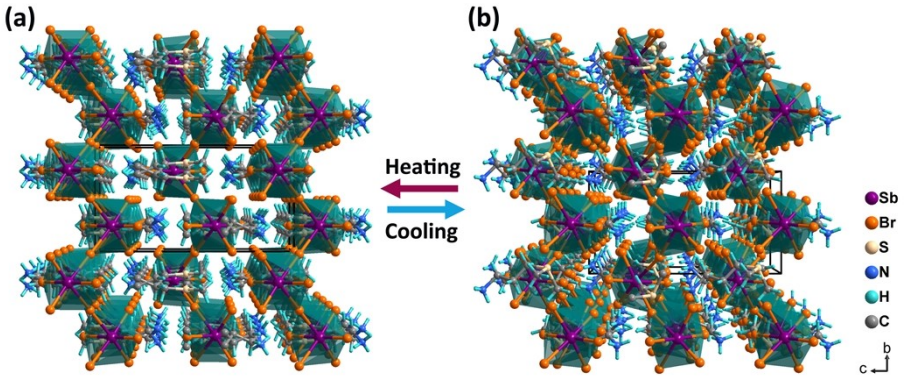

Fig. S4 The packing diagrams of **1** at 303 K (a) and 100 K (b).

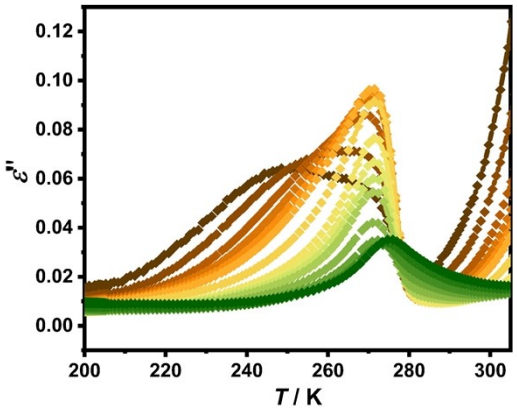

Fig. S5 The imaginary part of the dielectric properties (ε'') of **1** at various frequencies from 1 kHz (dark red) to 1000 kHz (green) in cooling process.

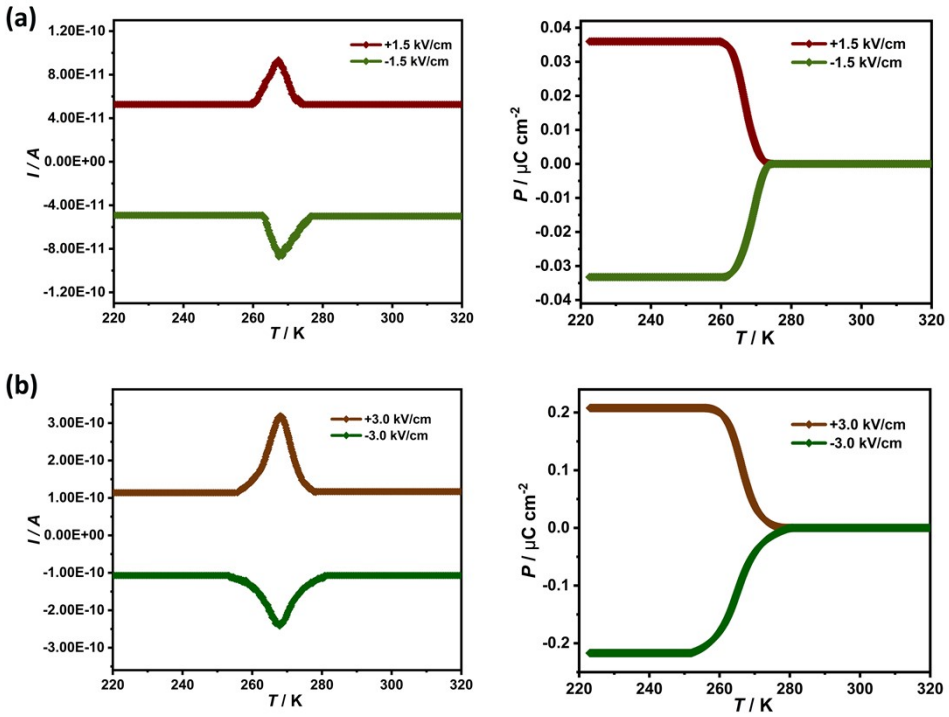

Fig. S6 The temperature dependent pyroelectric current and spontaneous polarization of **1** at different poled voltages of about ±1.5 kV cm^{-1} (a) and 3.0 kV cm^{-1} (b), respectively. By integrating the pyroelectric current with respect to time, spontaneous polarizations(*P*) of about 0.036 μC cm^{-2} (a) and 0.21 μC cm^{-2} (b) were obtained.

Reference

1. W. Kohn and L. J. *Sham, Phys. Rev*, 1965, **140**, A1133.
2. W. Jia, J. Fu, Z. Cao, L. Wang, X. Chi, W. Gao, and L. W. Wang, *J. Comput. Phys.*, 2013, **251**, 102.
3. A. V. Krukau, O. A. Vydrov, A. F. Izmaylov and G. E. Scuseria, *J. Chem. Phys.*, 2006, **125**.
4. J. P. Perdew, K. Burke, and M. Ernzerhof, *Phys. Rev. Lett*. 1996, **77**, 3865.
5. P. Ziesche, S. Kurth, and J. P. Perdew, *Comput. Mater. Sci.*, 1998, **11**, 122.
6. H. J. Monkhorst and J. D. Pack, *Phys. Rev. B*, 1976, **13**, 5188.